ORNL/TM-5514

FFM Water Mockup Studies of the Near-Wake Region of Permeable Flow Blockages

John D. Sheppard

OAK RIDGE NATIONAL LABORATORY
OPERATED BY UNION CARBIDE CORPORATION FOR THE ENERGY RESEARCH AND DEVELOPMENT ADMINISTRATION

DISCLAIMER

Printed in the United States of America. Available from
the Energy Research and Development Administration,
Technical Information Center
P.O. Box 62, Oak Ridge, Tennessee 37830
Price: Printed Copy $4.00 ; Microfiche $2.25

ORNL/TM-5514
Dist. Category UC-79,
-79e, -79p

Contract No. W-7405-eng-26

Engineering Technology Division

FFM WATER MOCKUP STUDIES OF THE NEAR-WAKE REGION OF PERMEABLE FLOW BLOCKAGES

John D. Sheppard

Date Published: October 1976

NOTICE This document contains information of a preliminary nature. It is subject to revision or correction and therefore does not represent a final report.

Prepared by the
OAK RIDGE NATIONAL LABORATORY
Oak Ridge, Tennessee 37830
operated by
UNION CARBIDE CORPORATION
for the
ENERGY RESEARCH AND DEVELOPMENT ADMINISTRATION

THIS PAGE

WAS INTENTIONALLY

LEFT BLANK

CONTENTS

FFM WATER MOCKUP STUDIES OF THE NEAR-WAKE REGION OF PERMEABLE FLOW BLOCKAGES

John D. Sheppard

ABSTRACT

An experimental study of transport in the near-wake region of permeable, planar flow blockages was conducted in a vertical-flow channel with a hexagonal cross section. Experiments included measurements of axial pressure distributions along channel walls exposed to the free stream and wake region and pressure differences between the free stream and wake regions at fixed axial positions. Further, time constants for scalar decay in the near-wake region were determined by salt conductivity tests. A single blockage geometry was used in all tests; the blockage, which was attached to the channel wall, obstructed 58% of the cross section when the blockage was solid. For one series of tests, discrete jets were machined into the blockage and water was metered into the recirculation zone at velocities of the order of the mean channel velocity. Increased jet velocity reduced the residence time of salt in the recirculation zone, and when the jet velocity was as high as the accelerated free stream flow at the vena contracta, counter-rotating cells were induced in the recirculating zone. In a second series of tests, uniformly spaced holes were drilled in the blockages to give blockage porosities of 11 and 24%. The residence time of salt in the near wake decreased significantly as the blockage porosity was increased to 24%.

INTRODUCTION

Studies conducted under the Fuel Failure Mockup (FFM) Program, which is part of the ORNL Liquid-Metal Fast Breeder Reactor (LMFBR) Safety and Core Systems Program, have comprised extensive experimental investigations

of effects of partial flow blockages on the thermal hydraulics of simulated LMFBR rod bundles.[1] Studies have been performed in the FFM Water Mockup which is a recirculating low-pressure water loop with a triple-scale 19-rod bundle.[3] The mockup has been operated primarily in support of the FFM sodium loop (engineering-scale 19-rod electrically heated bundle). Due to the relative ease of operation of the water mockup, tests have covered a wide variety of test conditions and have included heat transfer studies with a single electrically heated rod,[3] hot-water injection tests, salt-tracer tests,[2] and flow-visualization studies.

Studies in both the FFM sodium loop and the water mockup have involved solid planar blockages obstructing up to 24 subchannels in the 19-rod bundles. The principal objective of these studies was to determine whether convective transport in the relatively stagnant recirculation zone (near-wake region) downstream of a blockage would be of sufficient magnitude to maintain acceptably low bundle coolant temperatures. It is notable that the FFM water mockup tests[3] and other analytical[4] studies suggest that a planar non-heat-generating blockage internal to a reactor core would have to obstruct a large fraction of the flow area, perhaps 50%, before temperatures in the wake region would reach the saturation temperature for sodium.

A first-order mixing model has been used to describe transport in the near wake downstream of rod bundle flow obstruction.[5] Such a model permits estimation of the mean temperature rise in the recirculation zone if the time constant for scalar decay, blockage or recirculation zone geometry, and fluid properties are known. Further, it has been shown that for typical ranges of flows in an LMFBR rod bundle, convective transport predominates

over conduction in the near-wake region.[5] Since convective effects predominate, data on mean residence time τ determined by salt-tracer tests in the water mockup can be readily used to estimate effects of blockages with liquid-metal coolants.

Mean residence time in the near wake behind solid planar blockages was reported[2] in dimensionless form, $T = \tau U/\ell_c$; U is the mean coolant velocity upstream of the blockage and ℓ_c is a characteristic length of the blockage. The parameter T was shown to be essentially independent of Reynolds number, $N_{Re} = \ell_c U/\nu$, over the range $10^4 < N_{Re} < 5 \times 10^5$, and when the characteristic length was the geometric mean of the largest blockage dimensions at right angles to each other, $T \simeq 10$ for central channel blockages and $T \simeq 26$ for edge blockages (no circulation past at least one side of the blockage). Further, it is notable that salt-tracer tests using blockages in the same flow channel without a rod bundle resulted in decreased residence time for both central and edge blockages, but the ratio $T_{edge}/T_{central} \simeq 3$ was about the same for tests with the rod bundle.[2]

Although initial water mockup experiments utilized solid blockages,[2,3] passage of coolant through a permeable blockage may have significantly different effects on wake region transport, depending partly on whether leakage is from an individual orifice discharging into the wake region or whether the blockage is rather uniformly permeable.

Gregory and Lord[4] cite unpublished experiments which suggested that flow through discrete orifices in blockages increased mixing in the near wake and therefore reduced the extent of temperature rise in the near wake. Calculations with their WAKE code[6] suggest that a 12% residual

flow through a central jet of an otherwise impermeable blockage significantly increases the turbulence level in the near-wake region, whereas 12% residual flow through a uniformly permeable blockage results in less turbulence.

Wind-tunnel studies by Castro[7] have shown that uniformly distributed flow through a central blockage tends to force the recirculation downstream of the blockage. When the blockage porosity was increased to about 25%, the recirculation zone detached from the blockage, thus resulting in a significant change in character of the near wake. Judd's[8] wind-tunnel experiments with permeable blockages in a rod bundle showed that the maximum turbulence level was in the shear layer emanating from the edge of the blockage. For a blockage with 12% porosity, the recirculation in the near wake was sufficiently strong that the turbulence was convected into the region immediately downstream of the blockage. However, for a blockage with 33% porosity, there was essentially no recirculation zone and a marked decrease in turbulence intensity in the near wake was noted. Turbulence measured immediately downstream of the blockage was attributed to that generated by shear flow through the blockage, since most of the turbulence generated in the outer shear flow was swept downstream.

The purpose of the study reported here was to explore some effects of permeable blockages. Two types of permeable blockage experiments were conducted in the FFM water mockup. For one series of tests, the blockages were fabricated so that water flow could be metered through discrete jets into the recirculation zone. Transport characteristics of the near-wake region were then studied as a function of the rate of discharge of fluid into the near wake. In the second series of tests, numerous uniformly

spaced holes were drilled in the blockages, and wake region transport was studied as a function of the porosity of the blockage. Since previous studies have shown similarities in transport effects in the recirculation zone with or without rod bundles, these permeable blockage experiments were conducted with no rod bundles.

EXPERIMENTAL EQUIPMENT

The water mockup is a recirculating-water loop consisting of a pump, a nominal 10-cm (4-in.) primary piping system, a test section, holding tanks, and flow-measuring instruments. The test section is a clear plastic flow channel with a hexagonal cross section (81 cm^2) oriented vertically for upward flow; the total test-section length is 1.4 m. Maximum water flow through the system is 0.32 m^2/sec (500 gpm), which corresponds to a maximum superficial velocity of 4 m/sec in the test section with no rod bundle. Instrumentation includes conductivity probes for monitoring the transient salt concentration in the test section and wall pressure taps for determining the axial pressure distribution.

Figure 1 shows the location of wall pressure taps in relation to a planar edge blockage that would obstruct 24 subchannels of the 19-rod triple-scale bundle[2] (1.73-cm rods on 1.24 triangular pitch). Pressure taps were located on the wall adjacent to the recirculation zone and spaced 2.5 cm apart for the first 20.3 cm downstream of the blockage then 5.1 cm apart to the end of the test section. Pressure taps are also located along the test section side opposite to the wake region taps (Fig. 1). These are referred to as free stream taps and are spaced on 12.7-cm centers upstream of the blockage at the same axial position as

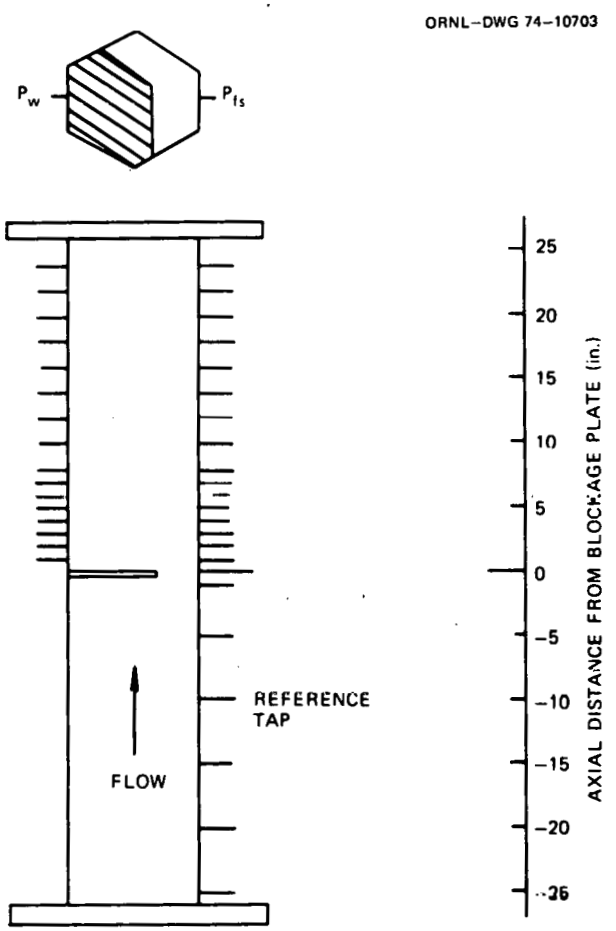

Fig. 1. Location of axial pressure taps in FFM Water Mockup.

the wake region taps downstream of the blockage. All pressures are differential measurements using oil and mercury manometers and are referenced to the free stream pressure 25.4 cm upstream of the blockage (Fig. 1). The conductivity probes were located in the walls adjacent to the near-wake zone 2.5 cm downstream of the center line of the blockage plate. Output from the conductivity circuit was monitored by a multichannel recorder at chart speeds which could be varied an order of magnitude (10 to 100 mm/sec), depending on the half-life of the salt concentration at a given flow rate.

Channel blockages were fabricated of 1.25-cm-thick phenolic laminated fabric that was both water resistant and easily machined. All planar blockages used in this study were equivalent in size and overall geometry to the 24-subchannel blockages used with the 19-rod bundle (Ref. 2, Fig. 35c). For solid blockages (no holes), approximately 58% of the channel cross section was blocked; the characteristic length, defined in previous studies,[2] was 8.15 cm.

SOLID BLOCKAGE STUDIES

Pressure drop measurements are particularly important, since the principal source of energy for transport in the recirculation zone is the permanent pressure loss associated with the blockage. Further, if the thermodynamic condition of the circulating fluid is near saturation, decreased pressure in the near wake due to flow acceleration past the blockage could result in boiling. Studies with the 19-rod bundle included pressure drop across the entire test section with and without blockages.[2] Although the data included entrance and exit effects, the pressure drop of the rod bundle alone was subtracted and a correlation presented for the effects of a planar blockage in a 19-rod bundle.

Preliminary to permeable blockage studies, axial pressure distributions along the test section were determined for mean channel velocities ranging from 0.46 to 3.05 m/sec with an equivalent 24-subchannel solid blockage. The blockage had the same geometry as that shown schematically in Fig. 1 and obstructed 58% of the channel cross sections. Typical axial pressure distributions are shown in Fig. 2 for velocities of 0.9 and 3.05 m/sec (3 and 10 fps). The circles indicate data from the free

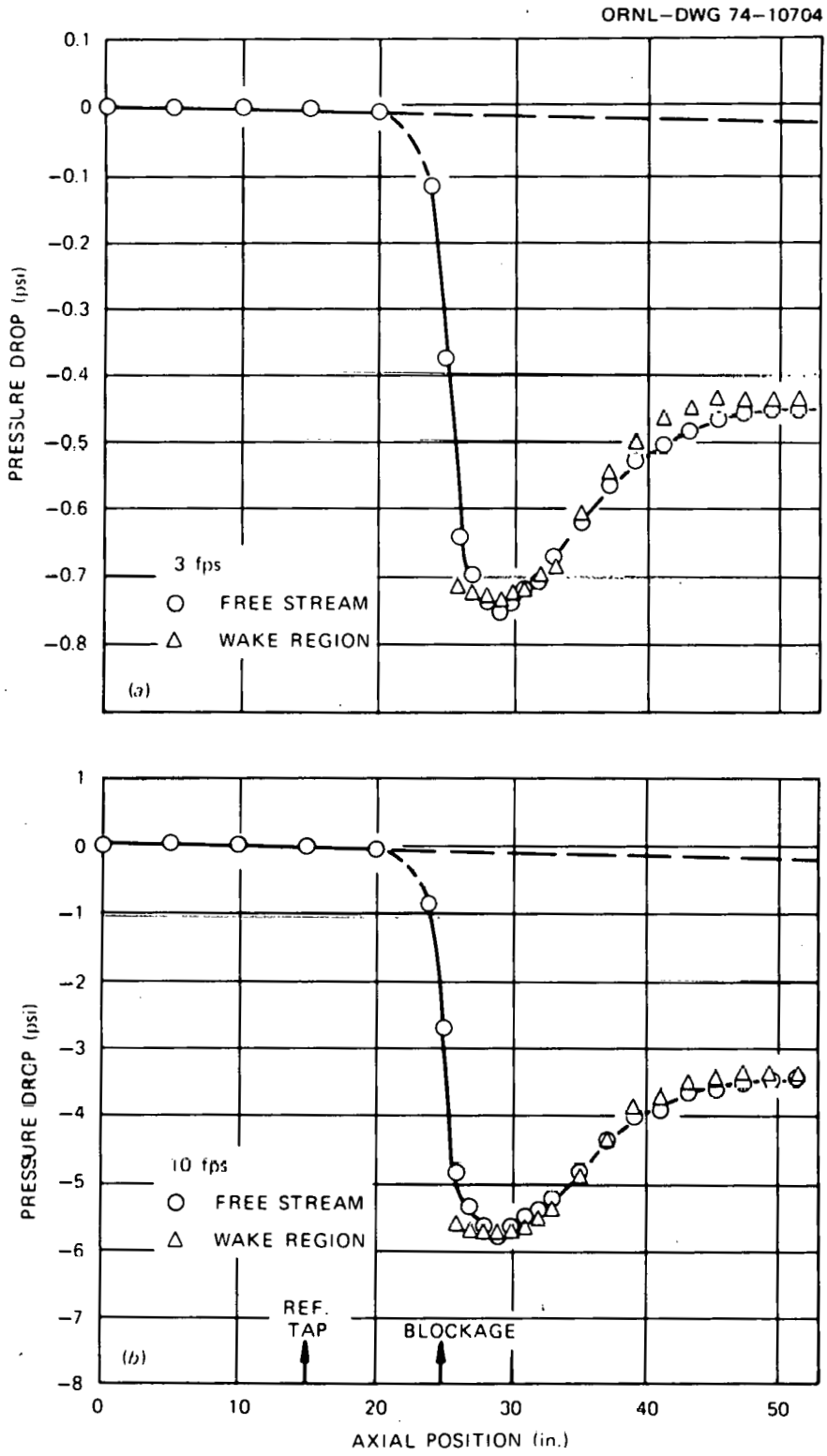

Fig. 2. Axial pressure distributions in FFM Water Mockup with a 24-channel edge blockage (no rods).

stream pressure taps, and the triangles are wake region pressures. All pressures are referenced to the pressure 25.4 cm upstream of the blockage plate.

The structure of the curves in the figure is typical of that for all the flows studied. Acceleration of flow past the blockage caused the pressure to decrease sharply to a vena contracta located approximately 10 cm downstream of the center plane of the blockage. Pressure recovery occurred in the region from about 10 to 51 cm downstream of the blockage. Over the range of flow studied, the permanent pressure loss was approximately 60% of the maximum, or the recovery factor was $\gamma = 0.4$. At the first axial position downstream of the blockage (2.5 cm), the pressure at the wall in the wake region was less than that of the free stream, and for a distance of 18 cm downstream of the blockage the pressure variation was less than about 5%.

The unrecovered pressure loss due to form drag was determined as the difference in unrecovered pressure and friction loss at a given axial position toward the end of the test section. Friction loss, which was relatively small compared to the total permanent loss, was estimated by extrapolation of upstream data into the wake region (Fig. 2).

The pressure loss due to the blockage is shown to be a function of the 7/4 power of channel velocity in Fig. 3. If the blockage Reynolds number is based on the characteristic length of the blockage, $N_{Re} = \ell_c U/\nu$, the pressure loss coefficient may be expressed as

$$\frac{\Delta P_B}{\rho U^2/2} = 113 N_{Re}^{-1/4} \quad . \tag{1}$$

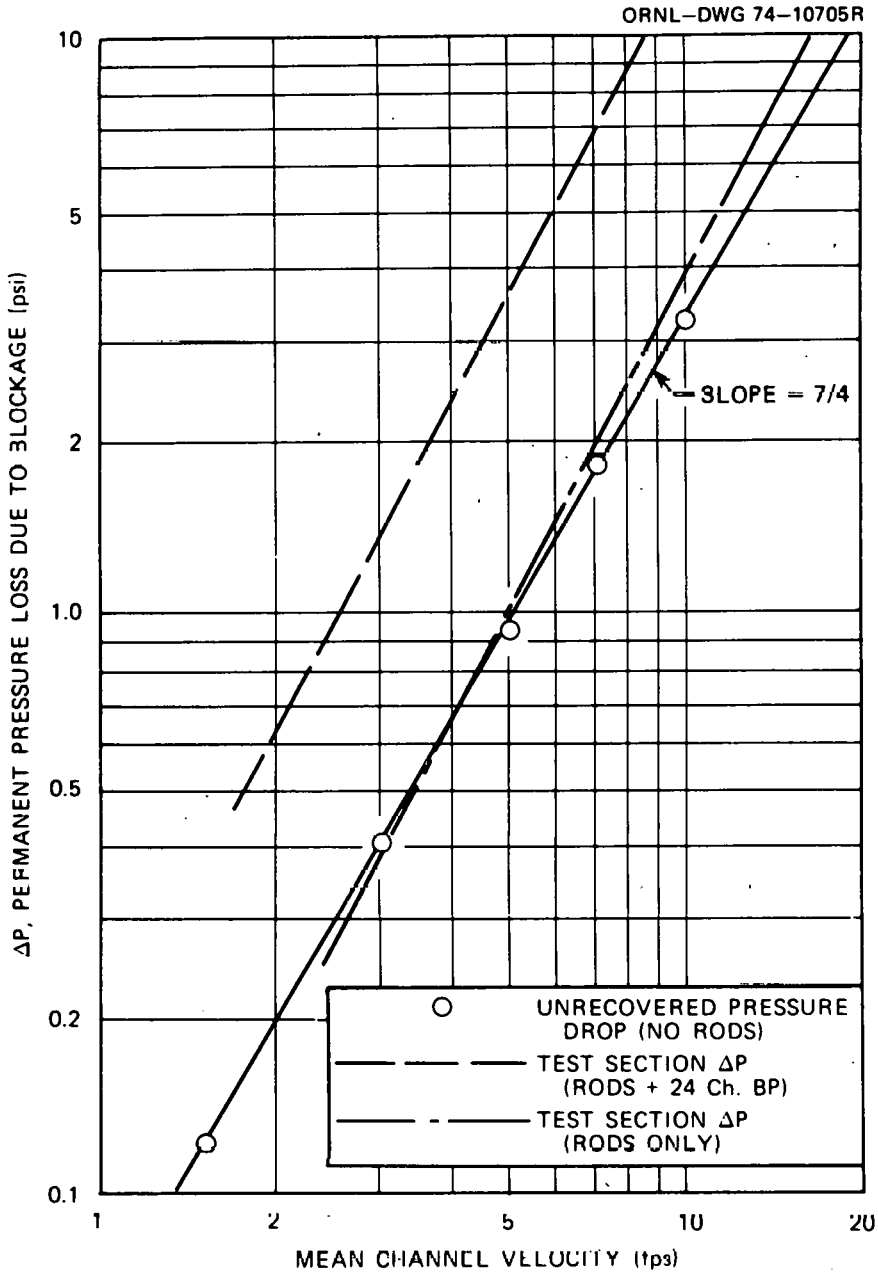

Fig. 3. Effect of velocity on permanent pressure loss due to a 24-channel edge blockage in FFM Water Mockup (no rods).

For example, when the mean channel velocity was 3 msec (10 fps), the loss coefficient was $\Delta P_B/\rho U^2/2 \simeq 5$, which is consistent with the range of coefficients reported, for example, by Smith.[9]

Figure 3 also shows the results of pressure-drop studies with a 24-subchannel blockage plate in the 19-rod bundle.[2] The line indicated by long and short dashes represents pressure drop with only the rod bundle in the test section, while the upper uniformly broken curve represents data with the rod bundle and the edge blockage plate. Note that the sum of the pressure loss of the blockage plate determined in this study with no rod bundle plus that of the rod bundle alone is significantly less than the total pressure drop across the rod bundle with the 24-channel edge blockage. For example, at a mean channel velocity of 1.5 m/sec, the sum of the pressure drop of the rod bundle and permanent loss of the blockage was approximately 13.8 kN/m^2 (2 psi) while the pressure drop of the test section with the rod bundle and blockage was approximately 24.8 kN/m^2 (3.6 psi). It must be emphasized that the rod bundle data were generated by two-point pressure-drop measurements, whereas data reported in this study were determined by axial pressure profiles. However, it is clear that the rod bundle affected the character of the wake region to the extent that the energy dissipation in the near wake was significantly increased.

In conjunction with axial pressure measurements, pressure differences across the channel at fixed axial positions ($P_{fs} - P_w$) were measured. Typical results are given in Fig. 4 for the same axial velocities as for the axial profiles shown in Fig. 2. When the pressure differences were normalized to the mean velocity head, the four sets of data were reduced essentially to a single curve; see Fig. 5. The pressure difference was

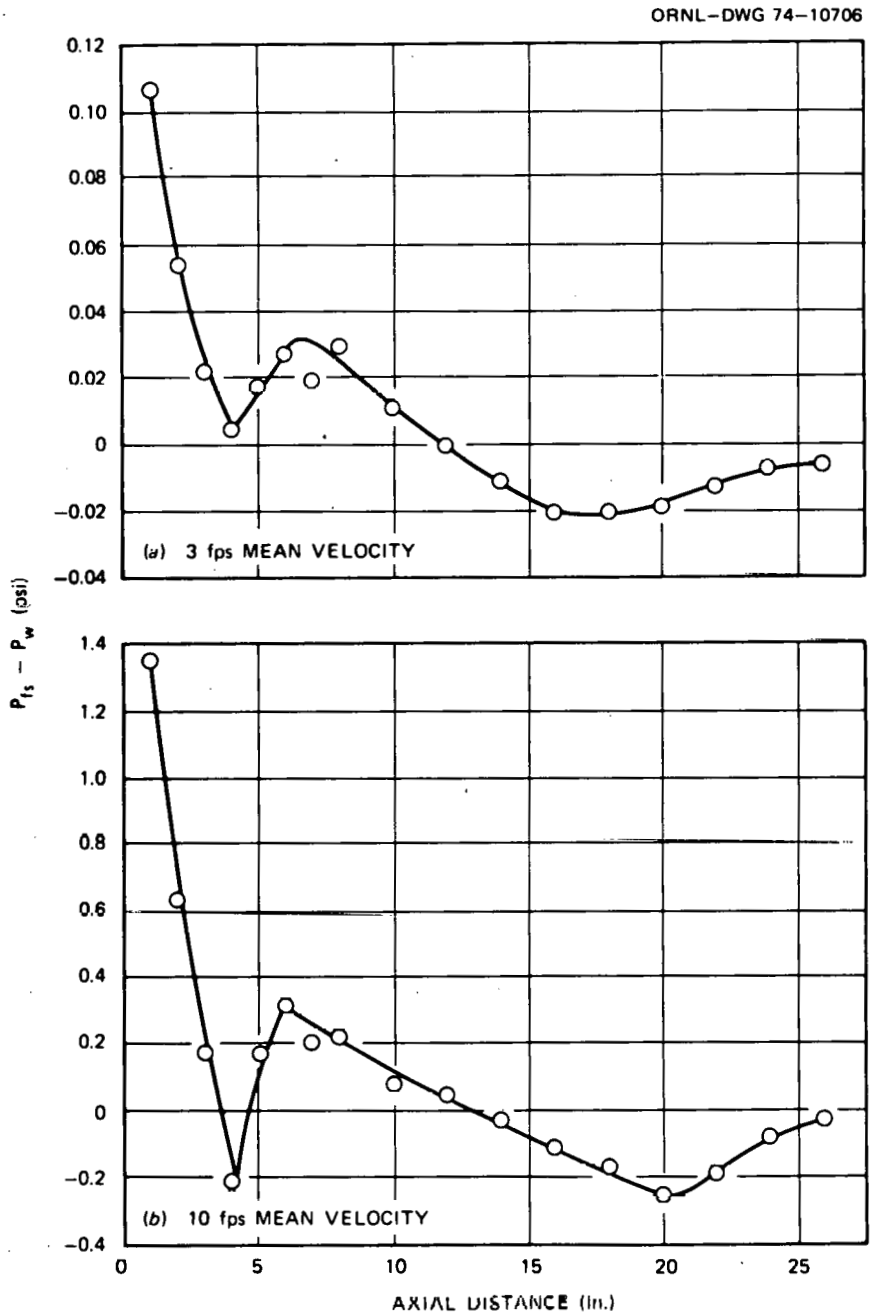

Fig. 4. Difference in free stream and wake region pressures as a function of axial position downstream of a 24-channel edge blockage (no rods).

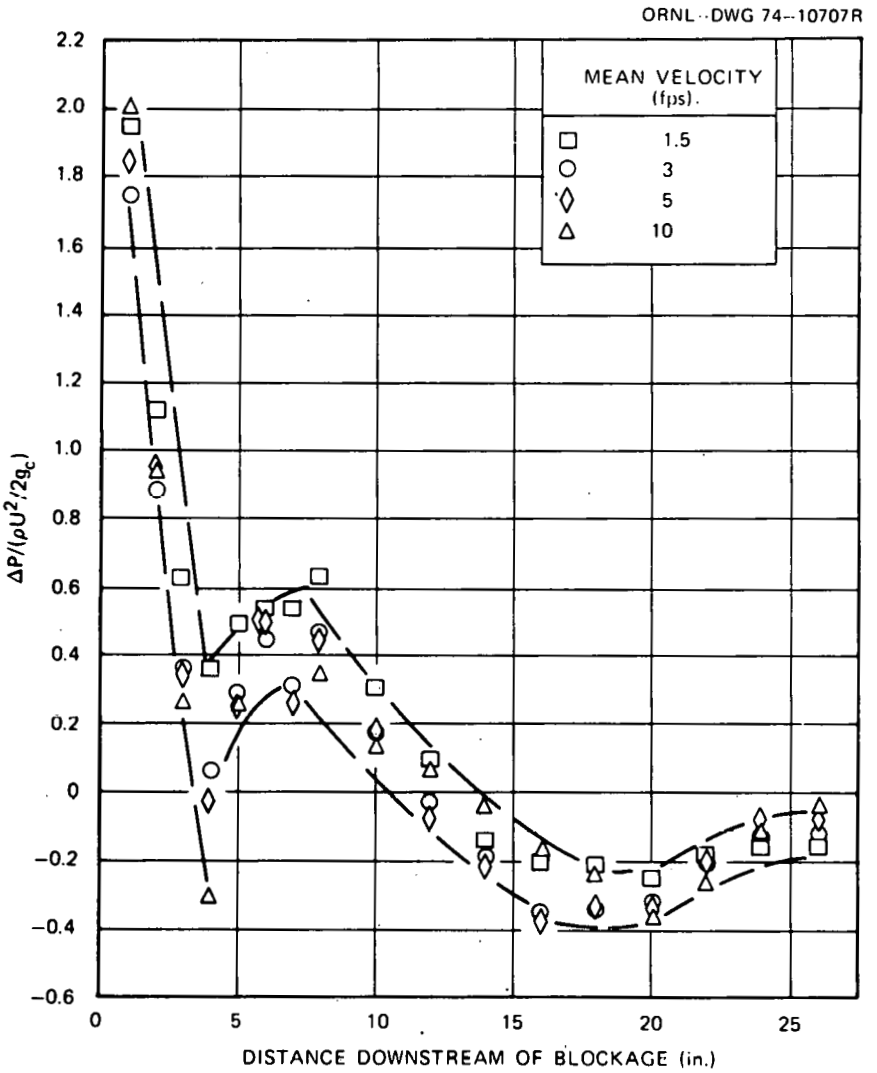

Fig. 5. Pressure difference across channel normalized to the mean velocity head as a function of axial position downstream of a 24-channel edge blockage (no rods).

always a maximum immediately downstream of the blockage, decreased to near zero at the vena contracta, and then increased to a relative maximum about 18 cm downstream of the blockage. Since the pressure along the wall of the wake region was relatively constant over this 18-cm span (Fig. 2), most of the variation in the pressure difference resulted from the initial acceleration and then deceleration of the free stream flow. From the

relative maximum, the difference decreased through zero to damped oscillations approaching zero at the end of the test section.

Wall pressure taps adjacent to the wake region were also utilized in a flow-visualization study of the length of the recirculation zone. Dye was injected through the pressure tap into the wake region. If the point of injection were clearly within the near-wake region, the dye was transported upstream toward the blockage. If the injection point were clearly downstream of the recirculation zone, the dye was rapidly swept downstream. The stagnation region was diffuse and variable, but the results of the test were quite useful.

Figure 6 shows the length of the recirculation zone normalized to the characteristic blockage length S/ℓ_c as a function of Reynolds number. The length S represents the distance along the wall at which transition from the recirculation zone to the stagnation region was observed. Typical test velocities in the water mockup range from 0.5 to 3 m/sec, and the blockage Reynolds number varies from about 4×10^4 to 2.7×10^5. Figure 6 shows that the length of the recirculation zone varies from about 30 cm at $N_{Re} = 4 \times 10^4$ to ~38 cm at $N_{Re} = 2.7 \times 10^5$. It is notable that this range of lengths of the near-wake region corresponds to the axial distances in Fig. 5 at which the pressure difference $(P_{fs} - P_w)$ is near zero; that is, at the stagnation (reattachment) region the pressure difference across the channel is near zero, although oscillations in Fig. 5 show that downstream of the stagnation point the pressure distribution is nonuniform.

The broken curve in Fig. 6 represents wake lengths determined by introducing air bubbles into the system upstream of the blockages and

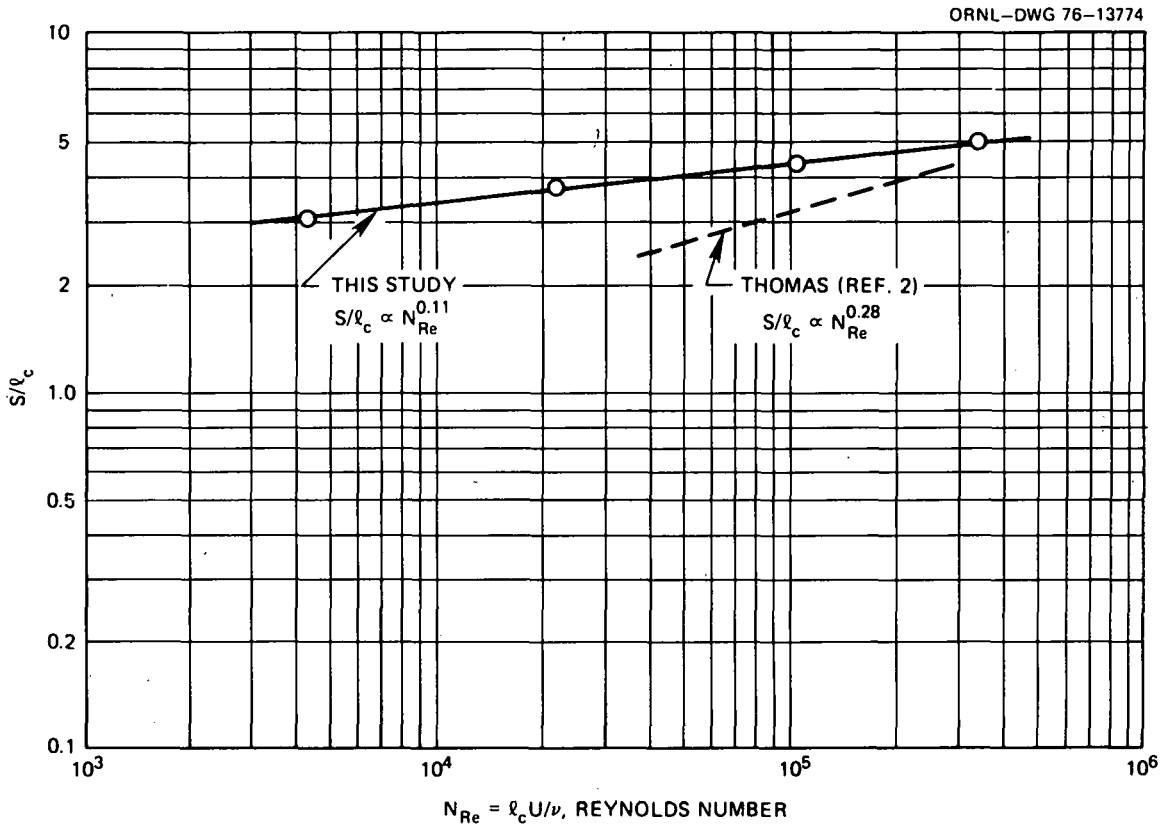

Fig. 6. Variation in near-wake length with Reynolds number as determined by dye injection at the wall adjacent to the recirculation zone (FFM Water Mockup; 24-subchannel edge blockage; no rods).

observing the trajectory of the bubbles in the recirculation zone.[2] These data show shorter wake lengths and a greater dependence on Reynolds number (a power law exponent of 0.28 compared to 0.11 for the dye study). It is notable that the two experiments were quite different; the bubble study considered a profile of the recirculation zone, while the dye study considered the character of the wall stagnation region. However, both techniques have been extremely useful in studying the character of the recirculation zone.

PERMEABLE BLOCKAGE STUDIES

Metered Leakage

Initial permeable blockage studies were concerned with the effects of a metered flow of water discharging into the recirculation zone from discrete jets on the downstream face of the blockage. An edge blockage equivalent to a 24-subchannel blockage in the 19-rod bundle was fabricated with a 0.64-cm-ID jet on the downstream surface so that the water would discharge into a relatively stagnant region of the near wake; see Fig. 7. The center of the jet was located 1.27 cm from the two nearest channel walls. The jet was connected through a test-section wall penetration

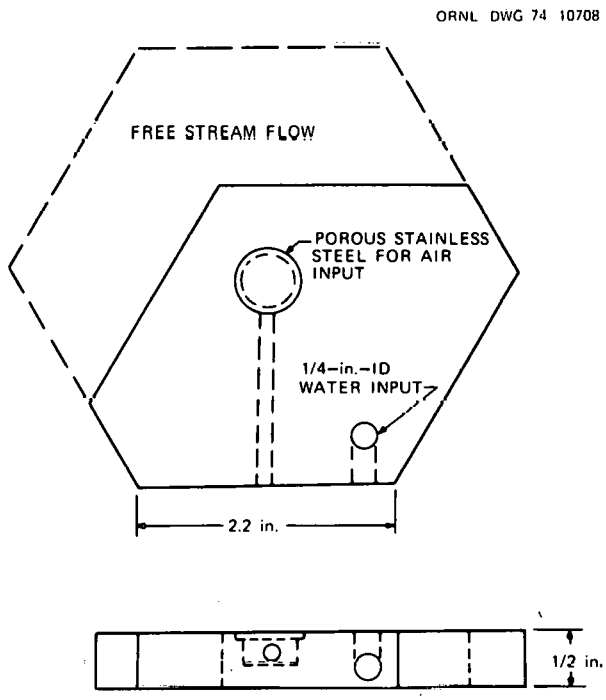

Fig. 7. Location of water and air inputs on leaky 24-subchannel edge blockage plate.

with a metered water supply with flow rates ranging from 0 to 1.3×10^{-4} m^3/sec, giving an average velocity of 0 to 4 m/sec in the 0.64-cm jet. Although fluid is added to the system through the jet, at the lowest channel velocity of 0.46 m/sec, the highest jet flow of 1.3×5^{-4} m^3/sec is less than 4% of the total channel flow. Therefore, the added mass above should not significantly influence hydrodynamics over a range of channel velocities from 0.46 to 3 m/sec. Figure 7 also shows a section of the blockage machined and fitted with a porous metal plate through which air could be dispersed directly into the wake region facilitating flow visualization studies.

Preliminary flow visualization studies were conducted at a mean channel velocity of 0.46 m/sec and mean jet velocities ranging from 0 to 1.8 m/sec. Using the characteristic length for this blockage as previously defined,[2] ℓ_c = 8.15 cm, the blockage Reynolds number at this channel velocity was $N_{Re} = \ell_c U/\nu \simeq 45{,}000$. Air injection through the porous disk in the blockage was maintained just high enough to observe flow patterns in the recirculation zone.

Primary flow patterns indicated by the air bubbles in the recirculation zone are shown in Fig. 8 for jet velocities of 0.46 and 1.74 m/sec (1.5 and 5.7 fps). The primary recirculation zone extended 20 cm (8 in.) downstream of the blockage, consistent with data of Thomas (Fig. 6) for wake length behind solid blockages at this Reynolds number. At a jet velocity of 0.46 m/sec, equal to the mean channel velocity, a secondary recirculation zone induced by the jet simply produced a minor inflection in the primary recirculation pattern (Fig. 2a). When the jet velocity was increased to 1.74 m/sec, two major recirculation zones resulted. The

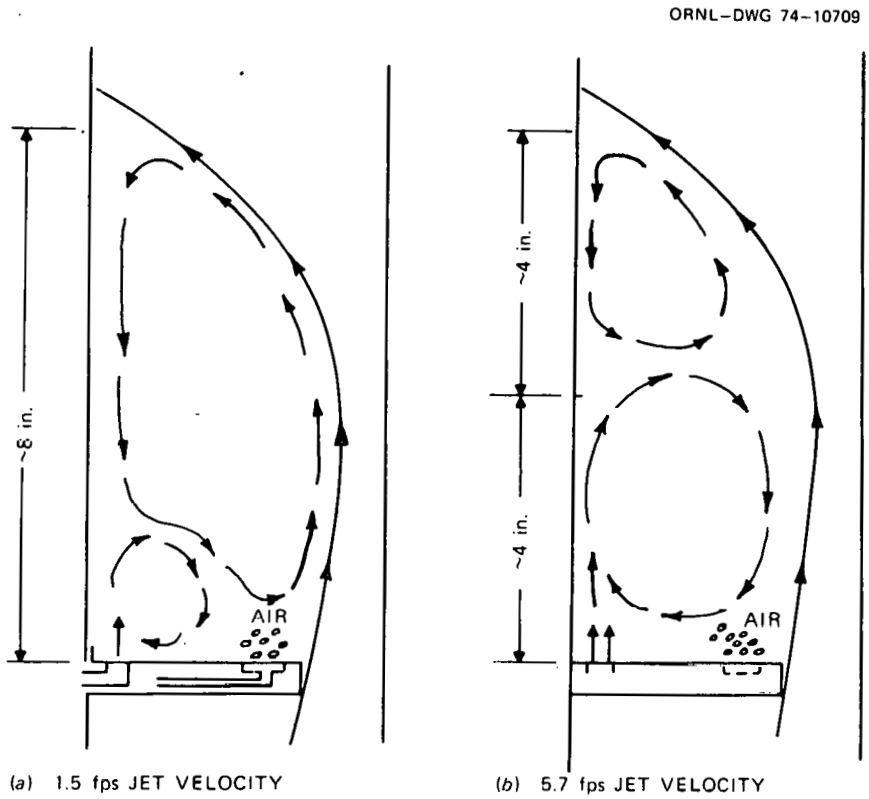

Fig. 8. Effect of jet velocity on the character of the recirculation zone behind a 24-channel edge blockage (1.5 fps unperturbed channel velocity).

zone adjacent to the blockage extended 10 to 13 cm downstream and the direction of circulation was controlled by the jet, that is, clockwise in Fig. 2a. The second recirculation zone was 7 to 10 cm long with circulation opposite to that of the first and with direction controlled by the free stream.

It is notable that the total length of the near-wake region was not significantly affected by the jet flow. Instead, the effect of increased jet velocity was to break the recirculation zone into two counter-rotating cells. At jet velocities greater than 1.74 m/sec, there was no observable

change in size of the two recirculation cells but their angular velocity visibly increased.

Axial pressure distributions under conditions similar to the flow-visualization studies are shown in Figs. 9 to 11; mean channel velocity was 0.46 m/sec and jet velocities were 0, 0.46, and 1.8 m/sec. When there

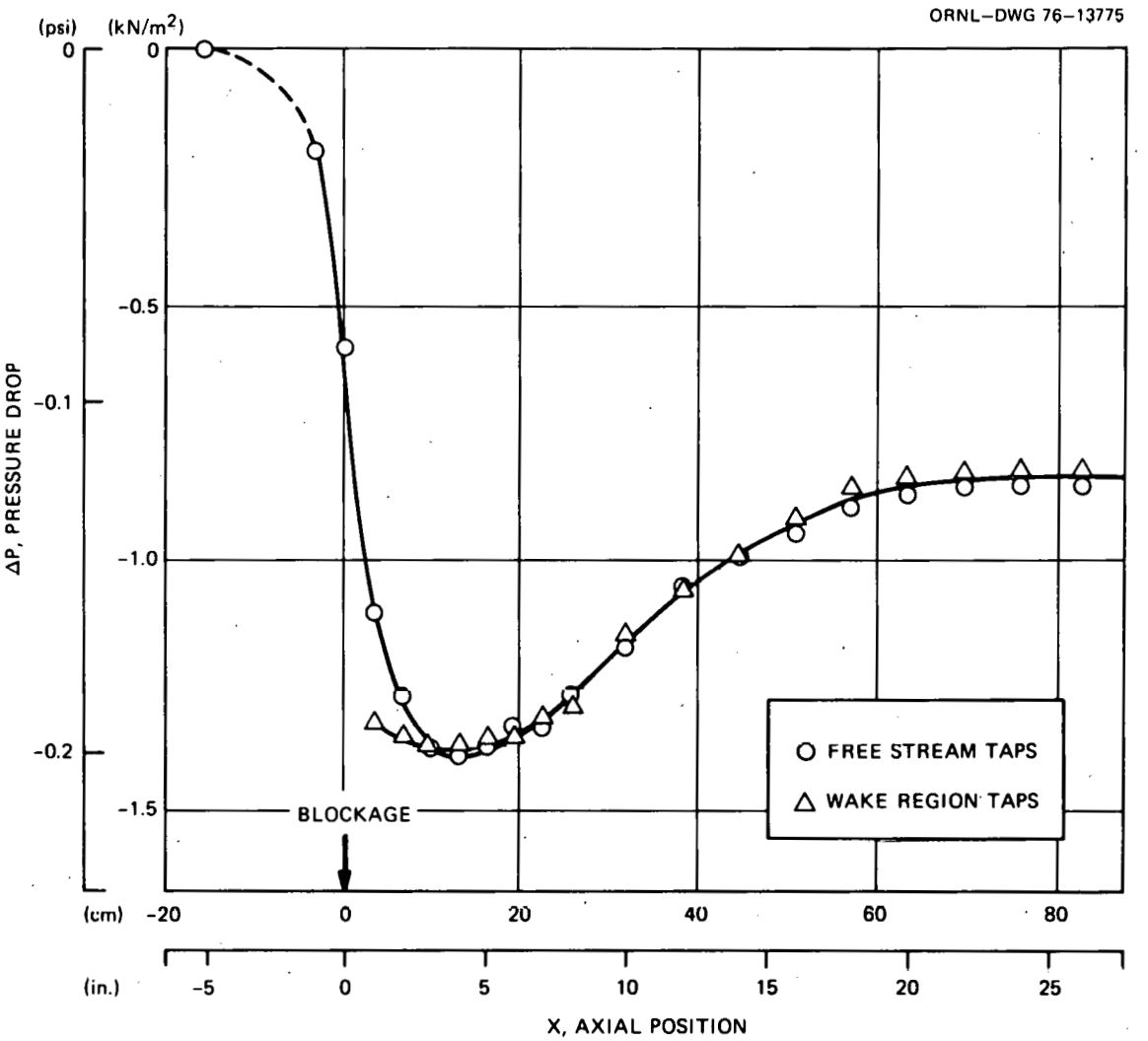

Fig. 9. Axial pressure distribution near a 24-subchannel edge blockage (FFM Water Mockup; no rods; 1.5 fps channel velocity; zero jet velocity).

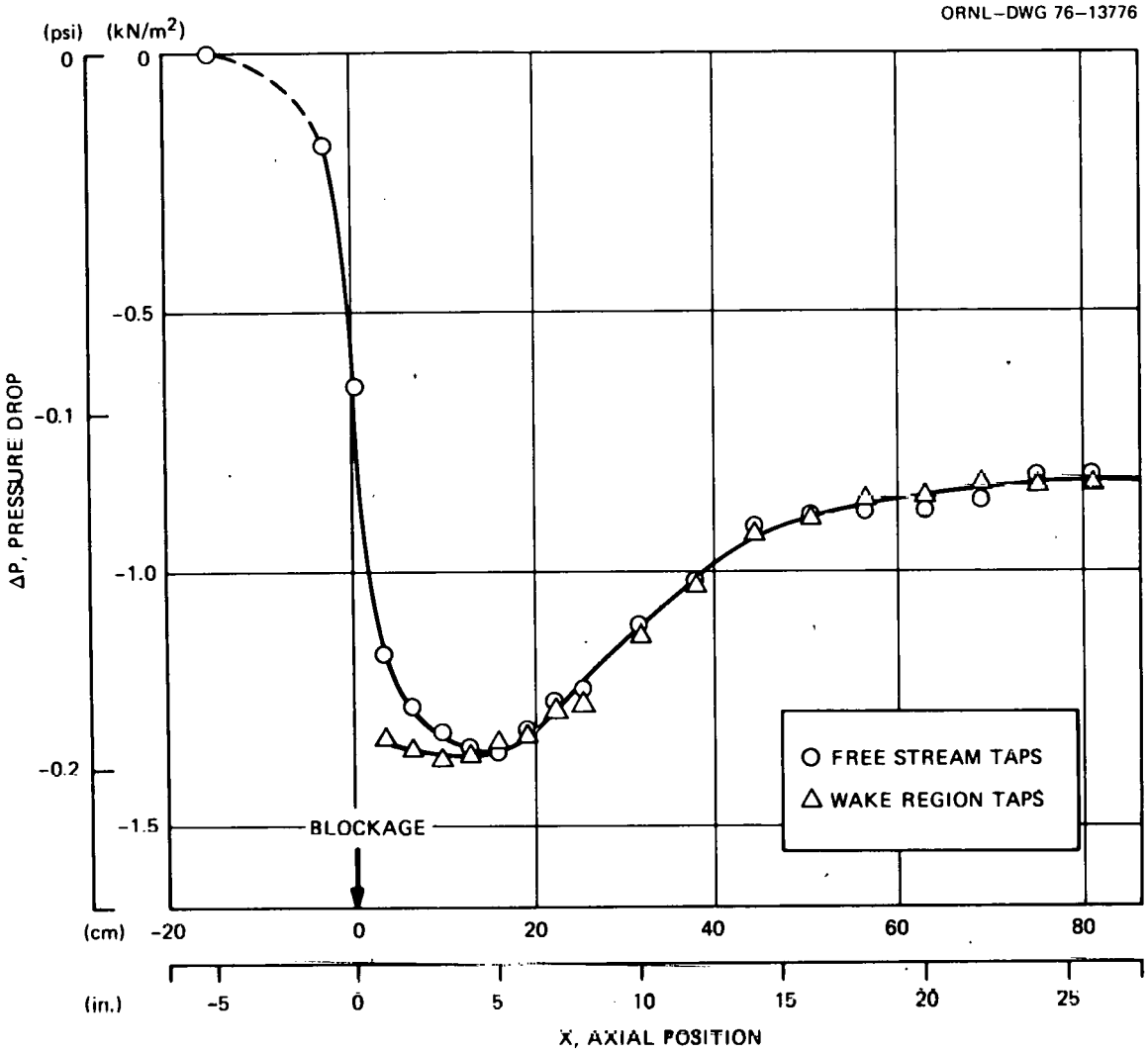

Fig 10. Pressure distribution in the vicinity of a 24-subchannel blockage with 1.5 fps velocity through a single 1/4-in. jet (1.5 fps channel velocity; no rods; FFM Water Mockup).

was no jet flow discharging into the recirculation zone (Fig. 9), acceleration past the blockage decreased the pressure to a minimum of 1.4 kN/m^2 relative to the pressure upstream of the blockage. The free stream pressure then recovered to give a permanent loss due to the blockage of about 0.83 kN/m^2. It is notable that the length of the recirculation zone determined by flow visualization to be ∿20 cm was near the beginning of

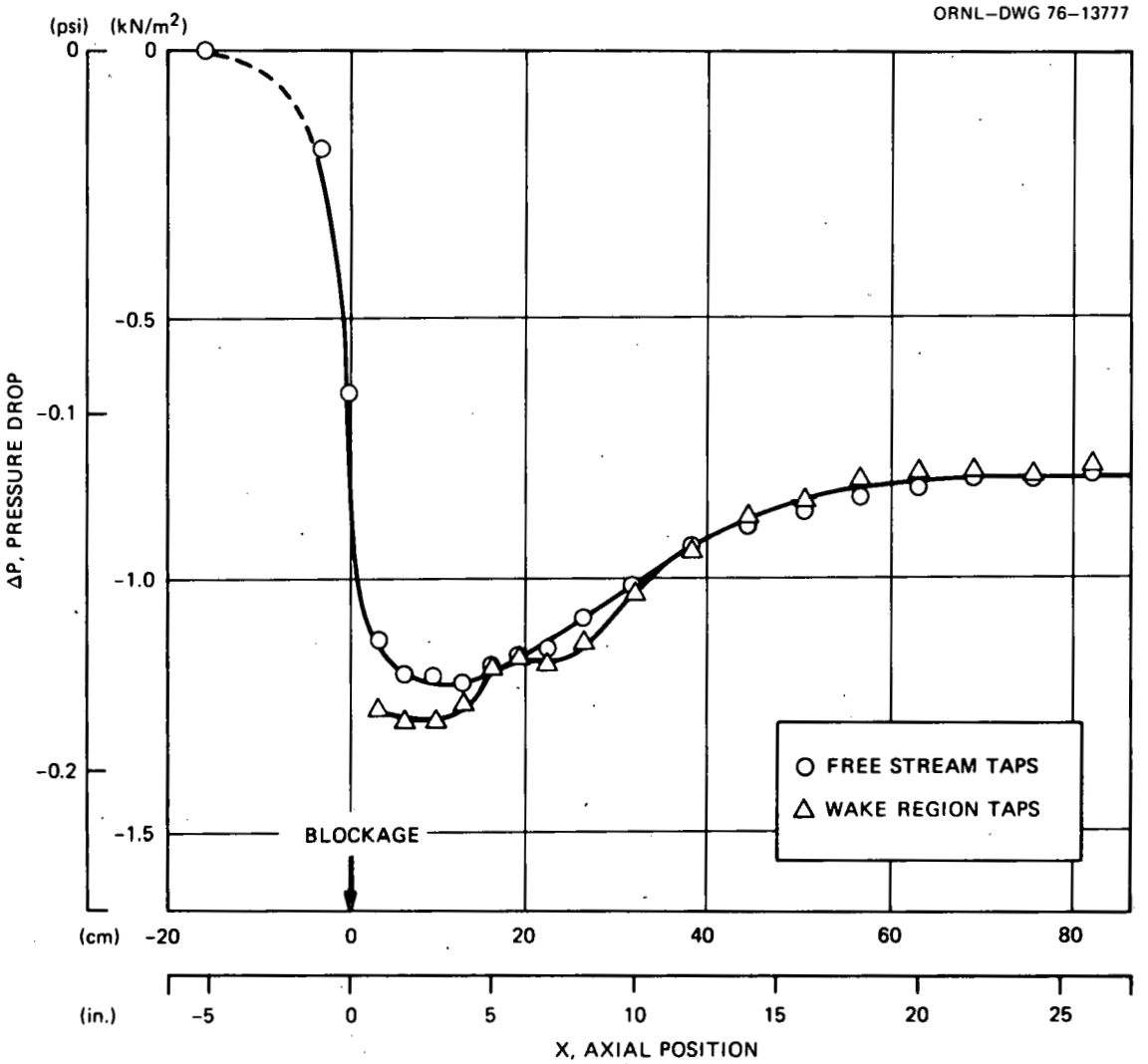

Fig. 11. Pressure distribution near a 24-subchannel edge blockage with 6 fps velocity through a single 1/4-in. jet (1.5 fps channel velocity; no rods; FFM Water Mockup).

rapidly recovering pressure but was far upstream of the region in which the pressure recovery was complete. When the jet discharge velocity was 0.46 m/sec, the pressure distribution was essentially the same as that with no jet (Fig. 10). However, at a blockage jet velocity of 1.8 m/sec, the wake region pressures show a distinct transition 10 to 13 cm downstream of the blockage. Further, the extent of the near-wake region (20 cm) is

readily associated in the figure with the axial position between the second pressure plateau ($\Delta P = -1.17$ kN/m^2) and the final rapid increase in pressure.

Comparison of the flow-visualization results (Fig. 8) and the pressure-drop results shows that the initial pressure plateau in the wake region corresponds to the clockwise rotation cell induced by the jet, and the second pressure plateau is characteristic of the counterclockwise cell controlled by the free stream. Use of the pressure-drop measurements and the Bernoulli equation provides an estimate of the free stream velocity at the vena contracta of the blockage with no jet to be 1.74 m/sec. The flow-visualization studies showed that the cell induced by the jet increased in size with velocity of the jet to finally dominate the recirculation zone immediately behind the blockage at a velocity of 1.74 m/sec. Further, its axial extent is approximately the same as the location of the vena contracta of the free stream. Thus, it appears that the extent of influence of this discrete jet was limited by the hydrodynamics of the free stream, namely the characteristics of the vena contracta.

Salt transport in the recirculation zone was also studied using conductivity probes in the wall adjacent to the wake region and located 2.54 cm downstream of the blockage. The technique was essentially the same as was used by Thomas.[2] A dilute solution of sodium nitrite was injected upstream of the blockage until the conductivity probes indicated that the recirculation zone was saturated with the salt. Injection was then stopped, and the decay of salt concentration was monitored by the conductivity probes. The half-life, $t_{1/2}$, of salt concentration in the wake was determined from the transient decrease in conductivity and was used to

calculate the time constant for scalar decay or mean residence time of salt in the wake according to first-order decay laws.[2,5]

Two different edge blockages were used in this study of effects of metered leakage rates on the wake region time constant. One blockage (Fig. 12a) was the same as that used in the flow-visualization studies and had a single 0.64-cm-diam (1/4-in.) jet. The second blockage had four 0.32-cm-diam (1/8-in.) jets distributed as shown in Fig. 12b; thus, for a given volume rate of leakage metered into the system, the mean velocity of jets of both blockages was the same.

The half-life of salt concentration in the wake region of both blockages is shown in Fig. 13 for mean channel velocities of 0.46 to 3 m/sec and leakage velocities up to 3.4 m/sec. When the mean channel velocity was 0.9 to 3 m/sec, there was no effect of metered leakage for either blockage over the range of leakage rates studied. When the channel velocity was 0.46 m/sec, the half-life of salt decay in the wake of the

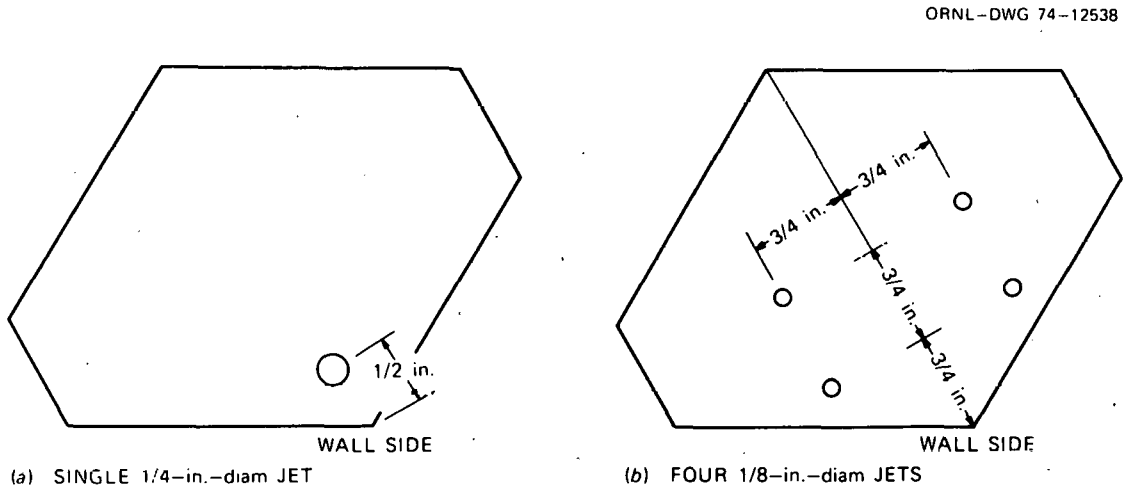

(a) SINGLE 1/4-in.-diam JET (b) FOUR 1/8-in.-diam JETS

Fig. 12. Location of jets for metered leakage experiments with 24-subchannel edge blockage (FFM Water Mockup).

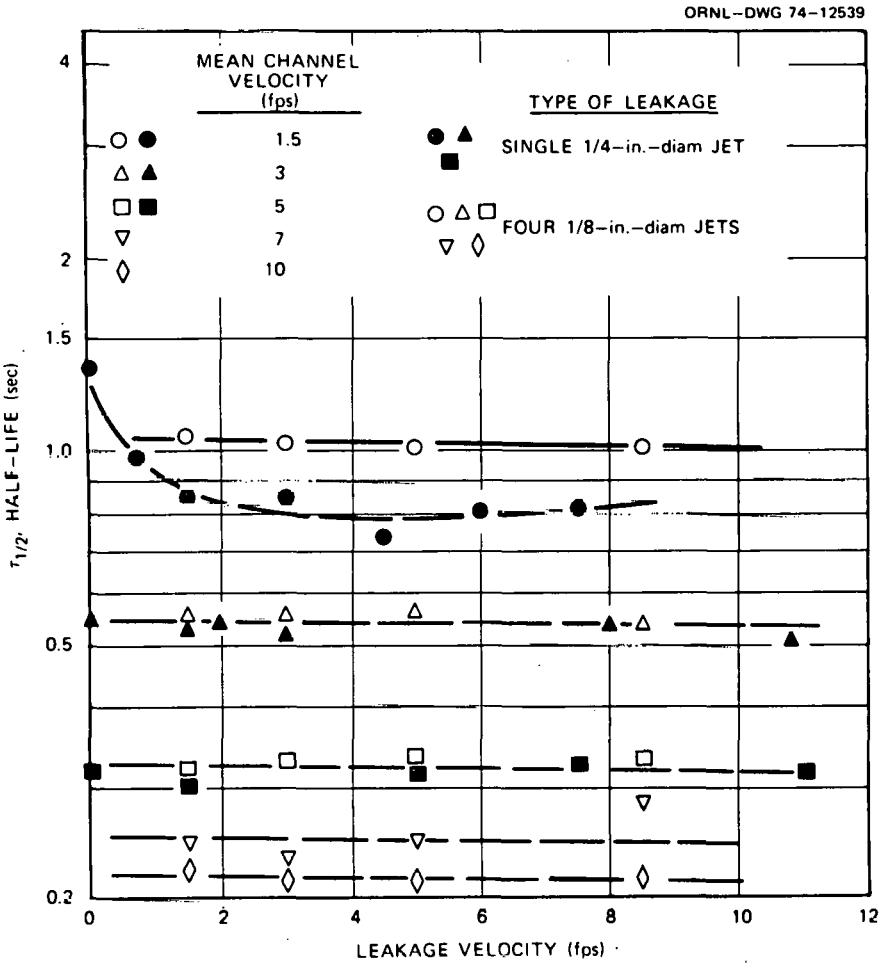

Fig. 13. Half-life of salt concentration decay in the near-wake region of edge blockages with measured leakage rates (FFM Water Mockup, 24-subchannel blockage, no rods).

four-jet blockage was also constant for jet velocities up to 2.6 m/sec. However, when the single-jet velocity was varied from 0 to 2.3 m/sec, the half-life decreased from 1.35 to 0.8 sec (solid circles in Fig. 6).

Figure 8 shows that at 0.46 m/sec channel velocity, the single jet included a secondary eddy that grew in size with increasing jet velocity until at 1.5 to 1.8 m/sec, the jet velocity in the near-wake region split into two counter-rotating cells. Apparently, the four 0.32-cm-diam jets

were so distributed across the blockage that when secondary eddies were induced they became too weak to have a major effect. Further, the recirculation zones associated with channel velocities of 0.9 to 3 m/sec were sufficiently strong so that the leakage jet into the wake region had no controlling effect.

Uniform Permeability

The second type of leaky blockage experiments concerned effects of uniform blockage permeability. Edge blockage plates (equivalent 24-subchannel blockages in the 19-rod bundle) were drilled through with 64 holes on a square pitch of 0.76 cm. One blockage had 0.318-cm holes, giving an open area of 24%. Wind tunnel studies[6] and computer simulations[4] have shown that detachment of the recirculation zone from permeable central blockages occurs at blockage porosities of about 20%.

Axial pressure distributions were determined for a solid edge blockage as well as for the two permeable blockages. The effect of leakage through the blockage on the pressure along an unblocked wall of the channel is shown in Fig. 14; mean velocity was 3 m/sec. Solid blockage data are the same as presented in Fig. 2. When there was no leakage through the blockage, the velocity continued to increase to a *vena contracta* located 10 cm downstream of the blockage. The effect of blockage porosity was to reduce the maximum pressure drop due to the blockage and to reduce the permanent pressure loss. At 11% porosity, the *vena contracta* was less distinct than that of the solid blockage and was located about 7.6 cm from the blockage compared with 10 cm for the solid blockage. The pressure distribution shows that when the blockage had 24% voids, acceleration of the free stream was essentially complete at the

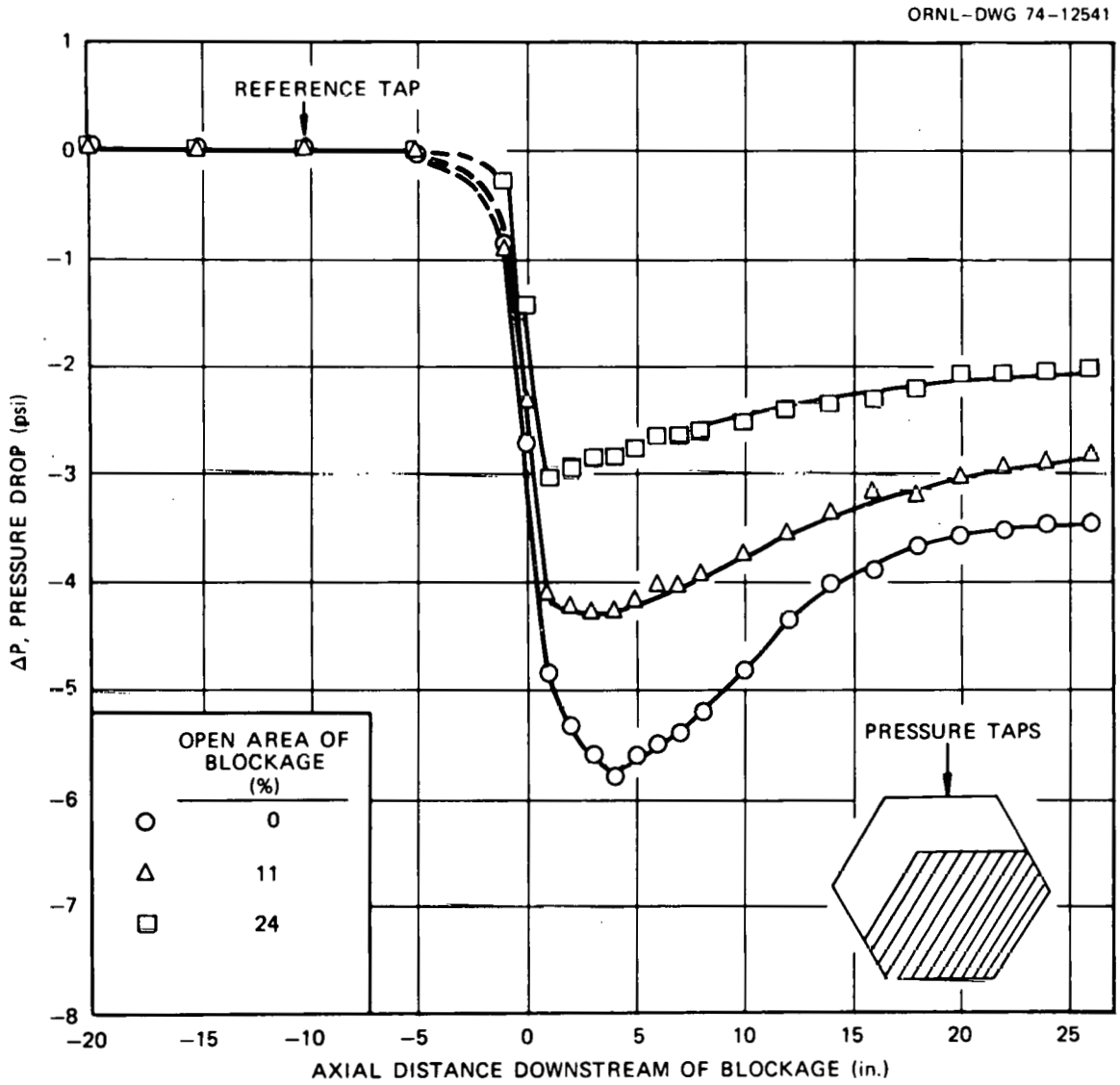

Fig. 14. Axial pressure distribution along a free stream wall of the FFM Water Mockup with permeable 24-subchannel edge blockages (no rods, 10 fps velocity).

plane of the blockage and the character of the wake region was distinctly different from that of the solid and 11% porosity blockages. This is consistent with results obtained using the WAKE code, which predicts that the recirculation zone "disappears" when the residual flow through the blockage is increased to about 20%. These results also complement the experiments

of Judd, who showed that while recirculation zones existed downstream of blockages with 0 and 11% porosity, the wake of a blockage with 33% porosity was a "largely featureless region."

Cross-channel pressure differences were also determined for the two porous blockages. Figures 15 and 16 show the data normalized to the mean velocity head superimposed on an outline of results of similar measurements with solid blockages (Fig. 5). Increased blockage porosity clearly

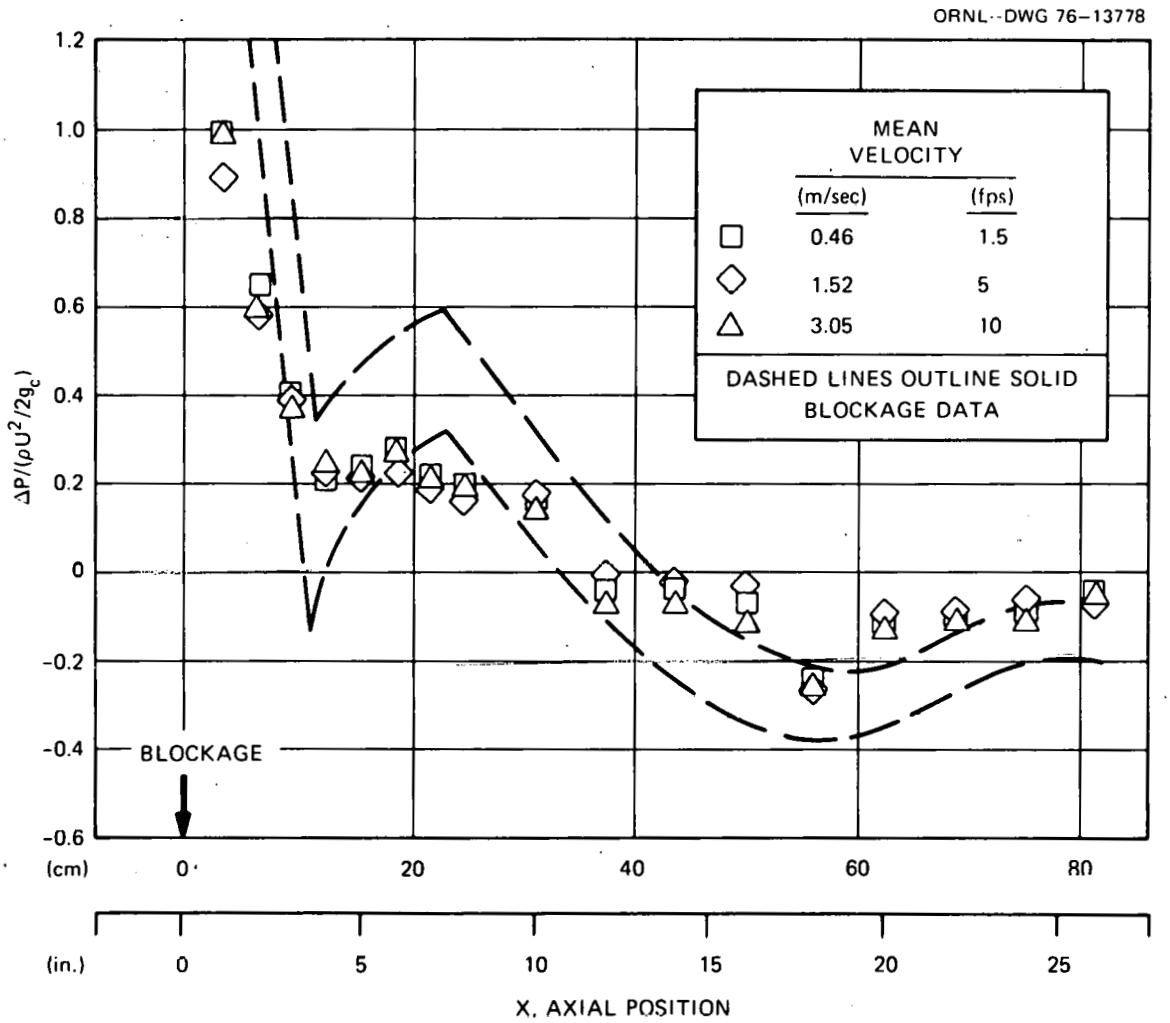

Fig. 15. Normalized pressure differences across the test section downstream of a 24-subchannel edge blockage with 11% voids (FFM Water Mockup; no rods).

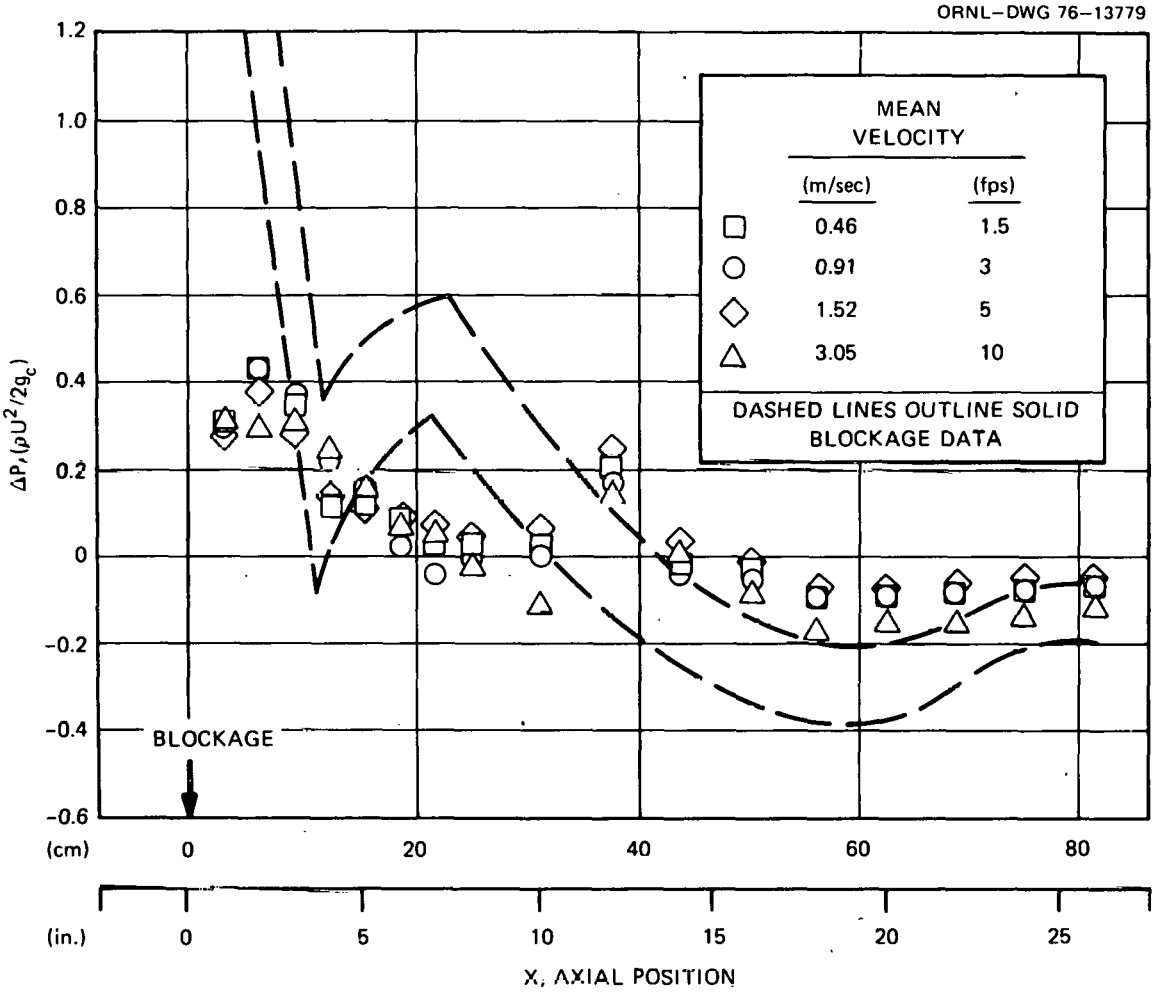

Fig. 16. Normalized pressure differences across the test section downstream of a 24-subchannel blockage with 24% voids (FFM Water Mockup; no rods).

resulted in deviations from profiles determined with the solid blockage. For example, immediately downstream of the solid blockage, the difference in free stream and wake pressures was approximately twice the mean channel velocity head, $\rho U^2/2$ (Fig. 5). However, the pressure difference at the same axial position and 11% voids in the blockage was only about one velocity head and for 24% voids was about one-third of a velocity head. Further, it is notable that increased blockage porosity decreased the

axial distance downstream of the blockage required to reduce the pressure difference to zero, which length was associated above with the length of the recirculation zone as determined by dye studies. That is, when the blockage had 24% porosity, the pressure difference measurements indicate that the near wake extended only 15 to 20 cm downstream of the blockage, which was nearly half that determined for the solid blockage for corresponding flow rates, 30 to 38 cm.

Salt concentration decay tests were conducted with no rods for both the 11% voids blockage (Fig. 17) and the 24% voids blockage (Fig. 18).

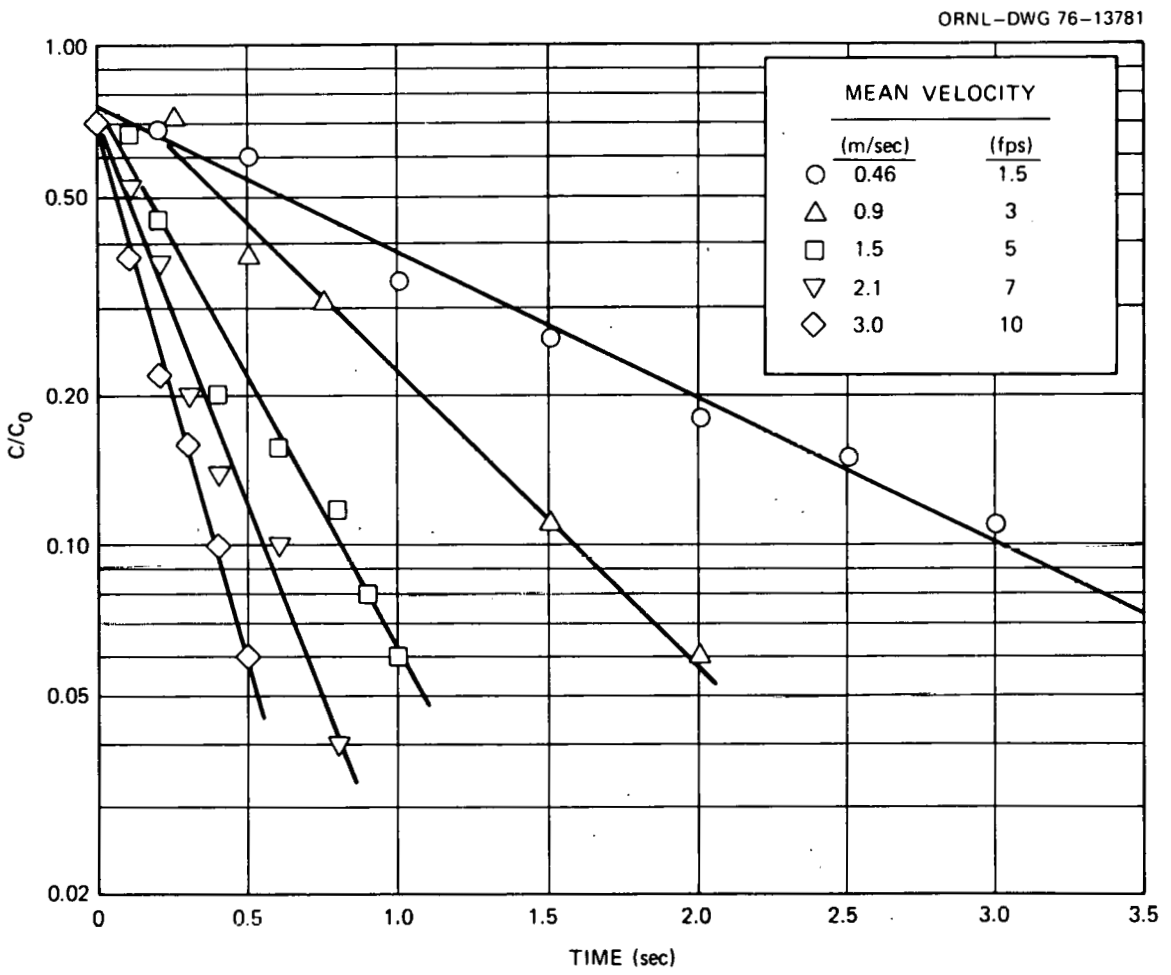

Fig. 17. Salt concentration decay in the wake of a 24-subchannel edge blockage with 11% voids (FFM Water Mockup; no rods).

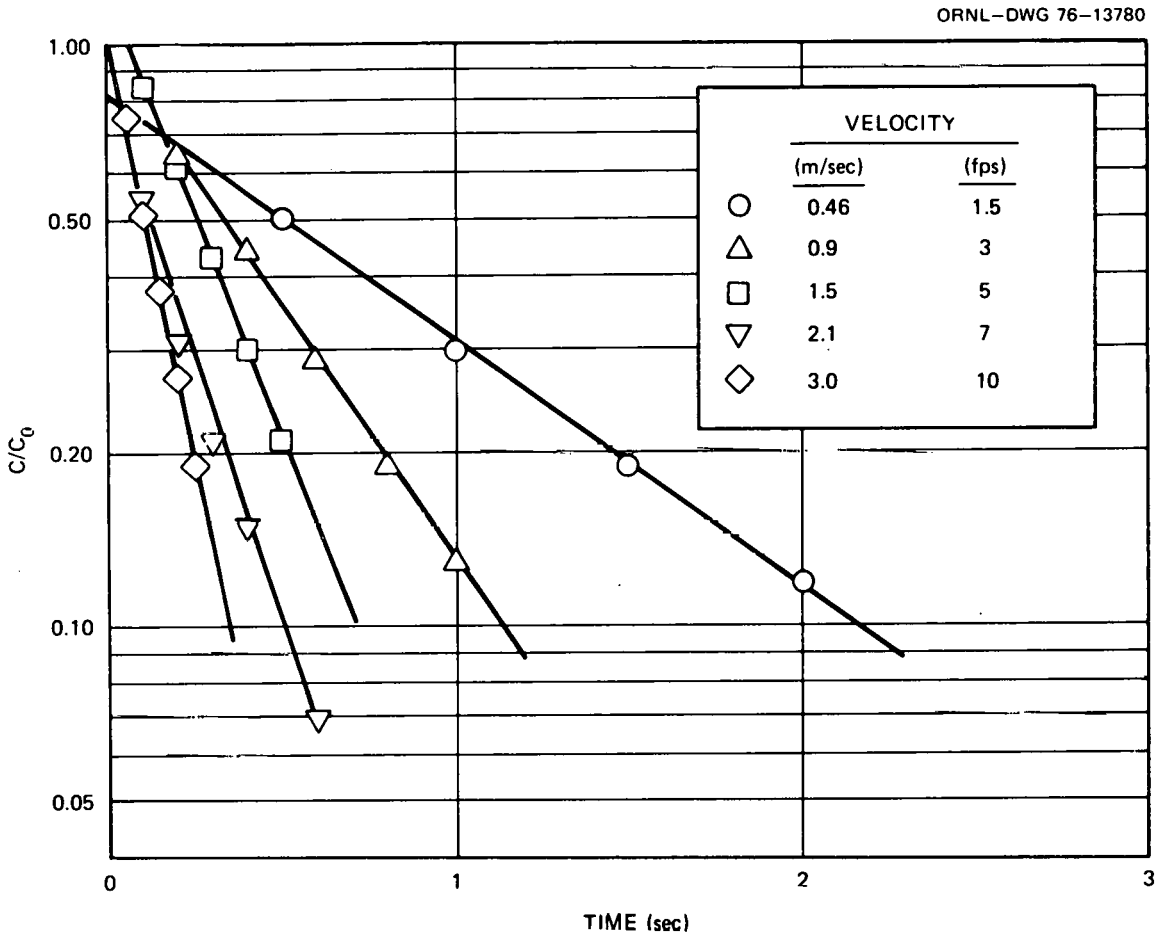

Fig. 18. Salt concentration decay in the wake of a 24-subchannel edge blockage with 24% voids (FFM Water Mockup; no rods).

Comparison of the slopes of the curves of the two figures for a given flow rate shows a marked reduction in half-life with the increase in porosity. Using the scalar decay time constant τ, mean velocity U, and characteristic blockage length ℓ_c, dimensionless time constants $T = \tau U/\ell_c$ were calculated for the two porous blockages and compared with results for solid blockages[3] (Fig. 19). The dimensionless time constants for the permeable blockages, like those for solid blockages, were essentially invariant with Reynolds number, $N_{Re} = \ell_c U/\nu$, over the range N_{Re} = 44,000 to 300,000. Further, the effect of increasing blockage porosity was to

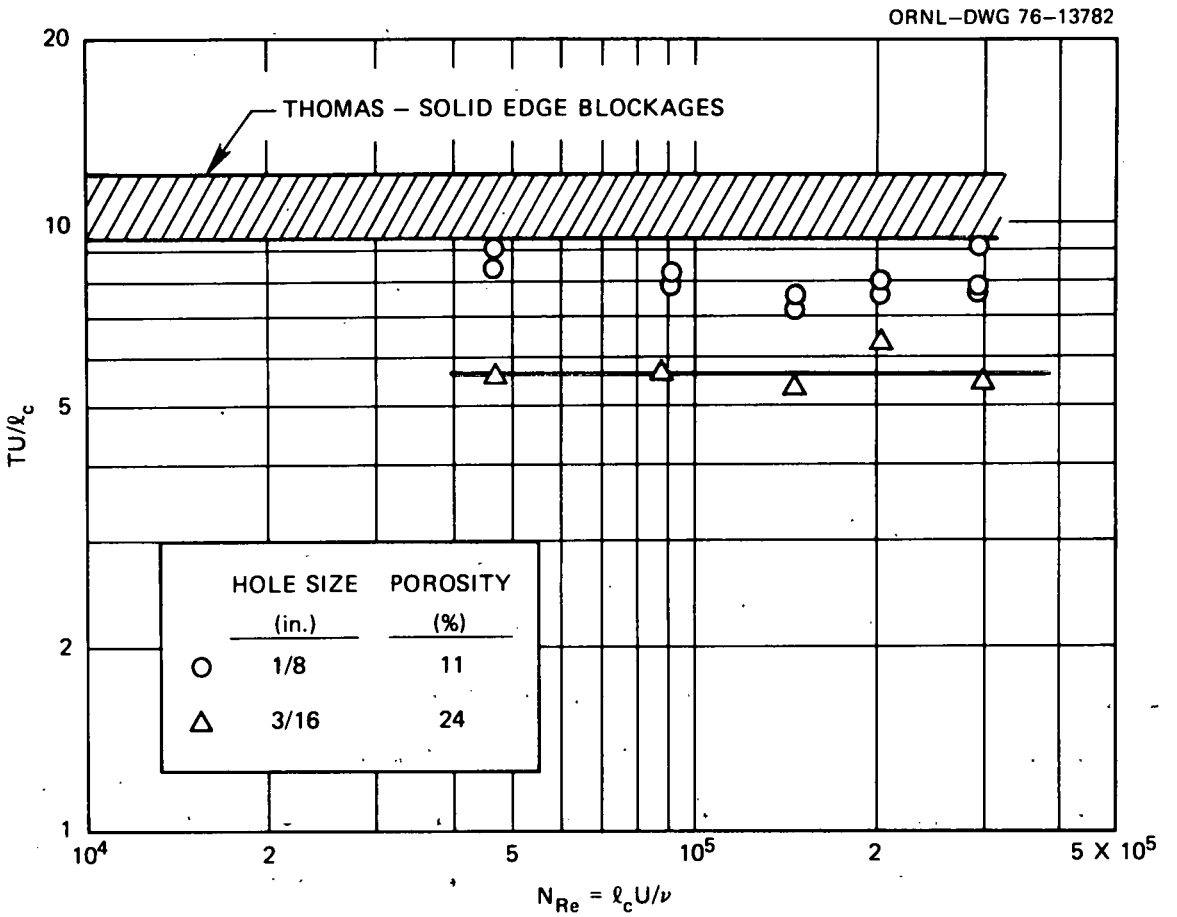

Fig. 19. Dimensionless time constants for salt concentration decay in the near-wake region of permeable 24-subchannel edge blockage (FFM Water Mockup; no rods).

reduce the mean scalar residence time from T = 10 for solid blockages to T = 8.5 for 11% porosity and T = 5.6 for 24% porosity.

TRANSPORT MODEL

The first-order mixing cell model offers a relatively simple estimate of the mean temperature increase in the recirculation zone downstream of a blockage in a heated rod bundle,[2,5]

$$\Delta\theta = \frac{\dot{Q}}{\dot{M}C_p}, \qquad (2)$$

where $\dot{Q}$ is the rate of heat production in the recirculation zone and $\dot{M}$ is the rate of transferral of mass from the zone. The mass flow is given by

$$\dot{M} = \rho V_r T \quad ,$$

where V_r is the volume of the recirculation zone. Equation (2) can be rewritten in terms of the near-wake volume and dimensionless residence time as

$$\Delta\theta = \frac{\dot{Q}}{V_r} \frac{T\ell_c}{\rho C_p U} \quad , \tag{3}$$

where $\dot{Q}/V_r$ represents the volumetric rate of heat production.

It is important to consider that transport of heat (or any scalar) out of the recirculation zone is not basically limited by resistance at the interface between the wake and free stream, but rather is a function of convection within the wake; that is, Prandtl (or Schmidt) number effects are insignificant. By factoring the near-wake volume into a characteristic area and length,

$$V_r = A_c S \quad , \tag{4}$$

where the area[10] is given by

$$A_c = C_v B_c^2 \quad , \tag{5}$$

the product of a form factor C_v and a characteristic diameter of the recirculation zone B_c, Eq. (3) can then be rewritten to define a recirculation zone Stanton number,

$$N_{St} \equiv \left(\frac{\dot{Q}}{A_c \, \Delta T} \right) \frac{1}{\rho C_p U} = \frac{S}{T\ell_c} \quad . \tag{6}$$

This Stanton number is a dimensionless measure of the rate of heat transfer

in the recirculation zone and should be a function of the coefficient of energy dissipation in the near wake,

$$f' = \frac{\Delta P \ell_c}{S\rho U^2/2} \quad , \tag{7}$$

where ΔP is the permanent pressure loss due to the blockage. Since Prandtl number effects are not important in this problem, it is suggested that for certain types of blockages (e.g., edge or central)

$$N_{St} \propto f' \quad , \tag{8}$$

similar to the Reynolds analogy, or

$$\frac{S}{T\ell_c} \propto \frac{\Delta P \ell_c}{S\rho U^2/2} \quad . \tag{9}$$

It is notable that both permanent pressure loss and wake length are functions of blockage size and coolant flow rate. However, both energy dissipation and wake geometry may be varied by modifications to a basic blockage size, for example, by changing the porosity as was done in this study. In such instances, Eq. (9) provides an estimate of the effects of blockage variations on the time constant. Table 1 summarizes calculations

Table 1. Transport and energy dissipation factors for planar permeable blockages in the water mockup [no rods; equivalent 24-subchannel blockage; 3 m/sec (10 fps)]

Blockage porosity (%)	Pressure loss, ΔP [kN/m^2 (psi)]	Wake length S [cm (in.)]	Dimensionless residence time T	N_{St} [Eq. (6)]	f′ [Eq. (7)]
0	24.1 (3.5)	38 (15)	10	0.46	1.11
11	20 (2.9)	30 (12)	8.0	0.47	1.15
24	14.5 (2.1)	20 (8)	5.6	0.45	1.25

of the wake region Stanton number and energy loss coefficient for the permeable blockage data presented above. Mean axial velocity was 3 m/sec. Dye study results (Fig. 6) were used for the near-wake length downstream of the solid blockage; the near-wake length for the porous blockage was determined from Figs. 15 and 16, since the axial distance at which cross-channel pressure differences were reduced to zero was associated with the near-wake length determined by dye studies. Table 1 shows that the Stanton number was essentially constant at 0.46 and the energy dissipation factor was $f' \approx 1.2$; thus $N_{St} \approx 0.38f'$.

Since the characteristics of the wake of a central blockage or blockages in rod bundles are different from the wake of these edge blockages, it is expected that the coefficient relating the energy loss factor to the Stanton number will differ somewhat from system to system. However, pressure-drop measurements and the simplified relationship of Eq. (9) should provide useful estimates of the mean transport characteristics in the near wake of a given system.

CONCLUSIONS

In all tests with edge blockages, flow into the near wake either by metered input or by flow through fixed blockage porosity always resulted in reduced time constants for scalar decay in the near wake. It is notable that the experiments of Judd showed that when the porosity of a uniformly permeable blockage was sufficiently high (33% compared to 12%), the recirculation zone disappeared and the turbulence level immediately downstream of the blockage was markedly reduced. This was interpreted as significantly increasing the near-wake temperature in an LMFBR rod bundle. However, in experiments similar to those of Judd, in that the character of

the wake bore distinct similarities, this study has shown that when blockage porosity was increased (25% compared to 11%) so as to eliminate the recirculation zone, the time constants for scalar decay of salt concentration markedly decreased. This result suggests that the mean temperatures in the wake of similar blockages in an LMFBR rod bundle would be reduced rather than increased.

It is significant that these tests utilized edge blockages so that flow around the blockages were not symmetrical. Further, in these studies considerable care was required to maintain a seal between the blockage and channel wall. Even small leaks at the wall markedly influenced wake region transport as was previously noted.[3]

Measurements of the pressure distribution in the vicinity of the blockage provide considerable information on wake geometry and transport characteristics. Laws of similarity can be utilized to extend pressure-drop results from a water to a sodium system. However, heater rods used in experiments with sodium coolants frequently warp,[11,12] resulting in a unique geometry for each rod bundle. Since the effect of warping on bundle hydraulics is not known in detail, it is recommended that pressure distributions be determined in these experiments as a diagnostic tool independent of the heat transfer studies.

NOMENCLATURE

A_c Characteristic cross-sectional area of recirculation zone

B_c Characteristic diameter of recirculation zone

C_p Heat capacity

C_v Form factor

f' Coefficient of energy dissipation

ℓ_c Characteristic blockage length

N_{Re} Reynolds number

N_{St} Stanton number

P_{fs} Free stream pressure

P_w Wake pressure

ΔP_B Total pressure loss due to blockage

$\dot{Q}$ Rate of heat production in recirculation zone

$\dot{M}$ Rate of mass transferral from recirculation zone

S Length of recirculation zone

T Dimensionless residence time

U Mean coolant velocity upstream of blockage

V_r Volume of recirculation zone

θ Temperature

ν Kinematic viscosity

ρ Density

τ Mean residence time

ACKNOWLEDGMENT

The author appreciates the fruitful discussions with D. G. Thomas during this study and the help of P. H. Hayes in conducting the experiments. M. H. Fontana made several useful suggestions in reviewing the manuscript, and Margie Adair typed the final manuscript.

REFERENCES

1. M. H. Fontana and R. E. MacPherson, Work Plan for LMFBR Fuel Failure Mockup Program, ORNL/TM-3902 (September 15, 1972).

2. M. H. Fontana et al., Thermal-Hydraulic Effects of Partial Blockages in Simulated LMFBR Fuel Assemblies with Applications to the CRBR, ORNL/TM-4779 (July 1975).

3. M. H. Fontana et al., Effect of Partial Blockages in Simulated LMFBR Fuel Assemblies, ORNL/TM-4324 (December 1973).

4. C. V. Gregory and D. J. Lord, "The Study of Local Blockages in Fast Reactor Subassemblies," J. Brit. Nucl. Energy Soc. 13, 251 (1974).

5. D. Kirsch and K. Schleisiek, "Flow and Temperature Distributions Around Local Coolant Blockages in Sodium-Cooled Fuel Subassemblies," in Progress in Heat and Mass Transfer, Vol. 7, O. E. Dwyer (Ed.), Pergamon Press, 1973.

6. C. V. Gregory and D. J. Lord, "Effect of Permeability on the Consequences of Local Blockages in Fast Reactor Subassemblies," J. Brit. Nucl. Energy Soc. 15, 53 (1976).

7. I. P. Castro, "Wake Characteristics of Two-Dimensional Perforated Plates Normal to an Air-Stream," J. Fluid Mech. 46, 599 (1971).

8. A. M. Judd, "Measurements in an Air Model of a Partly Blocked Fast Reactor Subassembly," J. Brit. Nucl. Energy Soc. 15, 47 (1976).

9. A. J. W. Smith, Pressure Loss in Ducted Flows, Butterworths, London, 1971.

10. G. Winterfeld, "On Processes of Turbulent Exchange Behind Flame Holders," Tenth Symposium on Combustion, p. 1265 (1965).

11. M. H. Fontana et al., Temperature Distribution in a 19-Rod Simulated LMFBR Fuel Assembly with an Edge Blockage (Out-of-Reactor Test for ANL FEFP P1 Experiment) - Record of Experimental Data for Fuel Failure Mockup Bundle 5A, ORNL/TM-4633 (November 1974).

12. M. H. Fontana and J. L. Wantland, LMFBR Safety and Core Systems Programs Progress Report for January–March 1975, ORNL/TM-4980 (November 1975).

THIS PAGE

WAS INTENTIONALLY

LEFT BLANK

ORNL/TM-5514
Dist. Category UC-79,
-79e, -79p

Internal Distribution

1. A. H. Anderson
2. M. Bender
3. J. R. Buchanan
4. R. M. Burnett
5. R. H. Chapman
6. W. H. Cook
7. W. E. Cooper
8. W. B. Cottrell
9. F. L. Culler, Jr.
10. R. G. Donnelly
11. G. G. Fee
12. W. F. Ferguson
13. G. F. Flanagan
14-18. M. H. Fontana
19. D. N. Fry
20. P. A. Gnadt
21. M. J. Goglia
22. A. G. Grindell
23. J. T. Han
24. N. Hanus
25. W. O. Harms
26. R. A. Hedrick
27. H. W. Hoffman
28. P. R. Kasten
29. T. S. Kress
30. R. Kryter
31. R. E. MacPherson
32. F. C. Maienschein
33. W. J. McCarthy
34. F. R. Mynatt
35. F. H. Neill
36. L. C. Oakes
37. L. F. Parsly
38. T. W. Pickel
39. H. Postma
40. J. P. Sanders
41. R. L. Scott
42. Myrtleen Sheldon
43-62. J. D. Sheppard
63. R. H. Sigler
64. M. J. Skinner
65. I. Spiewak
66. J. J. Taylor
67. D. G. Thomas
68. R. H. Thornton
69. E. T. Tomlinson
70. D. B. Trauger
71. J. L. Wantland
72. J. R. Weir
73. J. S. White
74. G. D. Whitman
75. W. J. Wilcox
76. M. C. Wynn
77-78. Central Research Library
79. Document Reference Section
80-82. Laboratory Records Department
83. Laboratory Records (RC)

External Distribution

84. Assistant Administrator for Nuclear Energy, Energy Research and Development Administration, Washington, D.C. 20545
85-86. Director, Division of Reactor Research and Development, Energy Research and Development Administration, Washington, D.C. 20545
87. Director, Reactor Division, ERDA, ORO
88. Director, Research and Technical Support Division, ERDA, ORO
89-330. For distribution as shown in TID-4500 under categories UC-79, -79e, -79p